Trans Indian Inst Met (2015) 68(Suppl 2):S243–S252
DOI 10.1007/s12666-015-0578-9

TECHNICAL PAPER

Gel-Combustion Synthesis of Nanocrystalline Cerium Oxide and Its Powder Characteristics

S. Balakrishnan[1] · D. Sanjay Kumar[1] · K. Ananthasivan[1]

Received: 1 December 2014 / Accepted: 12 May 2015 / Published online: 2 June 2015

Abstract Nanocrystalline ceria powders were prepared by using citrate gel combustion. The influence of the composition of the combustion mixture on the characteristics of the final product was investigated. Ceria powders obtained by calcining the combustion residue in air at 1073 K were characterized for their specific surface area (SSA), X-ray crystallite size (XCS), bulk density (BD), particle size distribution (PSD) and residual carbon. The dependence of these properties on the fuel to oxidant ratio (R) of the initial mixture was investigated. The microstructure of the calcined ceria powders prepared from a mixture with R = 0.25 was investigated by using high resolution transmission electron microscopy. All the calcined powders were pelletised and sintered at 1473, 1673 and 1873 K, and their sinterability was compared by measuring the density of the sintered pellets. A maximum sintered density of 98 % theoretical density could be achieved at a temperature as low as 1473 K for the first time for the powder prepared from a mixture with R = 0.75. The systematic dependence of the properties of these powders on the composition of the initial mixture is being reported for the first time. Powders obtained from a mixture with an R value 0.25 showed a linear increase in sintered densities with the sintering temperature. Other powders exhibited anomalous decrease in the sintered density at high temperature, probably due to irregular grain growth coarsening.

Keywords Ceria · Citric acid · Combustion synthesis · Nanocrystalline · Sintering

1 Introduction

Cerium oxide (CeO_2) is an important binary oxide that finds applications that ranging from its use as a three way catalyst (TWC) in automobile exhaust [1], to a solid electrolyte in solid oxide fuel cell (SOFC) [2–4]. The oxygen non-stoichiometry exhibited by this oxide owing to the multiple valence states of cerium renders it suitable for gas sensing [1, 5]. Studies on this oxide are of interest to the nuclear industry for cerium oxide could serve as a surrogate for PuO_2 owing to its chemical similarity to the latter [6, 7]. Further it is one of the important fission products that are found in significant quantities in the irradiated nuclear fuel.

Studies on the synthesis and sintering of ceria in general and nanocrystalline ceria in particular are relevant to the above applications. Many methods have been used to prepare nanocrystalline ceria that include solution combustion synthesis [1], sol–gel processing [8], hydrothermal [9], mechanochemical [10], sonochemical [11] and co-precipitation [12] syntheses.

Among the above mentioned methods, combustion synthesis is a simple and cost effective method for preparing nanocrystalline cerium oxide with desired material properties [13–18]. This method is particularly advantageous owing to its simplicity, low cost, reproducibility and control over the stoichiometry [13–18].

✉ D. Sanjay Kumar
sanjaypch08@gmail.com

S. Balakrishnan
balakrish@igcar.gov.in

K. Ananthasivan
asivan@igcar.gov.in

[1] Advanced Fuel Studies Section, Fuel Chemistry Division, Indira Gandhi Centre for Atomic Research Kalpakkam, Chennai, Tamilnadu, India

The properties of the nanocrystalline oxide powder obtained through the combustion synthesis could be tailored by varying the composition of the combustion mixture comprising a fuel (usually an organic compound) and an oxidant (metal nitrate). The fuel as well as the composition of the starting mixture is an important parameter in the combustion synthesis. Chandramouli et al. [19] reported that the citrate-gel combustion proceeds through a reaction which is moderate unlike the combustion involving urea. Nanocrystalline powders of urania, thoria and solid solutions of urania and ceria and many rare earths have been successfully synthesized [7, 19–21] in our laboratory through this procedure. The investigations reported in the references [17, 22–25] describe the strategies adopted by different authors for arriving at the optimum composition of the combustion mixture. Jain et al. [26] suggested a novel thermo chemical method for calculating the stoichiometric fuel to oxidant ratio for an exothermic reaction.

Very recently, Banerjee and Devi [25] and Haribabu et al. [14] have investigated the combustion synthesis of nanocrystalline ceria by using a mixture of fuels. When binary fuel mixtures are used usually the one with a higher heat of combustion (glycine) and another with a lesser heat of combustion (citric acid) are used in order to control the exothermicity of the reaction [17, 22–25]. Hwang et al. [15] synthesized ceria in bulk quantity through a "dry powder" method and obtained a product with a high carbon residue. In this method urea was used as the fuel and a violent reaction was reported. Yuan [27] proposed the use of an alcohothermal method in the presence of poly(vinylpyrrolidone) as the stabilizer. This method could not be scaled up for it is expensive and involves more number of steps. Xu et al. [24] synthesized yttria doped ceria by using a fuel mixture comprising citric acid and ammonium nitrate. These authors did not attempt to optimize their method. Purohit et al. [16] synthesized nanocrystalline ceria by using glycine as the fuel. However, these authors did not carry out any investigation on the systematic dependence of the properties of the product on the composition of the combustion mixture.

Recently, Biswas and Bandyopadhyay [28–30] have proposed the use of urea–formaldehyde gel combustion method for synthesizing doped nanocrystalline ceria powders. Optical properties of these powders obtained through the above said method were strongly influenced by the concentration of the dopants (La^{3+}, Pr^{3+} and Nd^{3+}).

Even though many authors had studied the preparation of nanocrystalline ceria by combustion synthesis, no studies have so far been reported on either the optimized conditions for the preparation or the sinterability of the powders obtained. Hence, in the present investigation, nanocrystalline ceria powders were synthesized by using the citrate gel-combustion. The effect of the composition of the combustion mixture on the properties of the powder was also studied.

2 Experimental Procedure

2.1 Starting Materials

Cerium nitrate hexahydrate of purity 99.9 % procured from M/s. Loba Chemie Pvt. Ltd., India and citric acid of purity 99.5 % was obtained from M/s. Merck (India) Ltd, Mumbai, India were used in this study.

2.2 Powder Synthesis

In a typical experiment, appropriate amounts of the oxidant (cerium(III) nitrate) and the fuel (citric acid) were weighed and dissolved in a minimum quantity of distilled water. This mixture was warmed on a hot plate in order to obtain a viscous gel. The ratio of the number of moles of the fuel (F) to that of the oxidant (O) was varied from 0.25 to 1.5 in steps of 0.25. The powders thus synthesized were called "as prepared" powders and these were calcined at 1073 K in air for 4 h in a furnace equipped with silicon carbide heating elements.

These samples were indexed as follows: "A" and "C" were used to designate the "as prepared" and "calcined" powders respectively. All these samples bore the prefix "CC" denoting cerium oxide prepared by using citrate gel-combustion, followed by numbers that indicated the fuel to nitrate ratio in percentage.

2.3 Characterization of the Reactants, Powders and Compacts

The purity of the starting materials was ascertained with the help of chemical assay by using inductively coupled plasma mass spectrometry (ICPMS model Elan 250 supplied by M/s. Sciex, Toronto, Canada). The IR spectra of the reactants and the products were recorded by using an ABB FTLA 2000 instrument. The bulk density of the "as prepared" and "calcined" powders was estimated from the weights of a known volume of these powders by using an electronic balance supplied by M/s. Scaltec, GmbH, Germany. Surface area of these powders was measured by using a Nelson–Eggertson type continuous flow apparatus supplied by M/s. Quantachrome Corp. Inc., USA (model: Monosorb). The X-ray diffraction patterns of the ceria powder samples were obtained by using an XPERT MPD X-ray diffractometer (M/s. Philips, The Netherlands). The average crystallite size of these powders was estimated by using the Scherrer as well as Hall Williamson methods. The latter revealed additionally the lattice strain in the crystallites. Standard single crystal silicon was used in order to correct the diffractograms for

instrumental broadening. The residual carbon present in these powders and sintered pellets was measured by estimating the amount of CO_2 that evolved during the oxidation of these samples. The size distribution of particles in the calcined powders was measured by using a particle size analyzer supplied by Mastersizer, M/s. Malvern Instruments, UK. The calcined ceria powders were compacted at 63 MPa in a double action hydraulic press supplied by M/s Bemco Hydraulics Ltd., Belgaum, India. These pellets were sintered in air at 1473, 1673 and 1873 K for 4 h at a heating and cooling rate of 300 Kh^{-1}. The densities of these sintered pellets were measured by using the liquid immersion technique, in which di-n-butyl phthalate was used as the pycnometric liquid. Microstructural characterization of the powders was carried out in a LIBRA 200FE (Carl Zeiss) high resolution TEM operated at 200 kV equipped with energy dispersive X-ray spectroscopy (EDS) analysis, scanning transmission electron microscopy (STEM) and an in-column energy filter. Samples for the microstructural analysis was prepared by dispersing a few milligram of CC025C sample in propan-2-ol followed by ultrasonication. A few drops of this solution were dropped on a holy carbon grid.

3 Results and Discussion

3.1 Assay of Ceria

The results obtained in the chemical assay of the cerium nitrate used in this study are given in Table 1. This indicates the presence of trace levels of rare earth elements like lanthanum, gadolinium, europium and ytterbium. Since the concentrations of these impurities are insignificantly low, their presence is unlikely to influence the sinterability of the final product.

3.2 The Gel Combustion Synthesis

The aqueous solution got dehydrated upon heating followed by frothing and finally the mass decomposed through a self sustaining reaction yielding the "as prepared" ceria powder. Since this reaction was carried out in an open glass bowl over a hot plate, the actual mean temperature of the reacting mass could not be reliably measured. The ceria powders obtained in this study were found to be granular and free-flowing. The relative proportion of the oxidant to the fuel in the combustion mixture was found to influence the combustion process as well as the characteristics of the product.

Two types of exothermic decompositions were observed during the combustion process, viz., one that was accompanied by a flame in the case of CC025A, CC050A, CC075A, CC100A and CC125A and another that was flameless (CC150A) that proceeded with smoldering. From these experiments it is evident that the duration of the combustion reaction increases with the value of R with an attendant reduction in the degree of exothermicity. In the mixtures with $R = 0.25$, the reaction was found to be most vigorous and the gaseous products were expelled from the reacting mass in a sudden bout resulting in spurting that threw the powder off the combustion bowl. The combustion reaction of both the mixtures with $R = 0.25$ and 0.50 yielded a fluffy and voluminous product. All the other mixtures exhibited reactions with moderate vigour and spurting.

The yellow color of these ceria powders deepened with the value of R between 0.25 and 1.00 and remained constant thereafter. The coloration was probably due to varying degrees of oxygen non-stoichiometry or due to color centers in the product. The lattice parameters of these powders did not evidence significant oxygen substoichiometry (Table 4; Fig. 4). Attempts were not made to determine the valence of cerium by measuring the resultant oxygen substoichiometry through chemical assay. However, the lattice parameters of these powders were estimated from their X-ray diffractograms.

3.3 IR Spectroscopy of the Reactants and Products

The infra-red spectra of the reactants and the product CC100A and CC100C are shown in Fig. 1. The presence of a weak absorption minimum at 1200–1700 cm^{-1} in the as-prepared powders could be attributed to the C–O stretch of the carbonate. A similar observation was reported by Haribabu et al. [14]. The absorption minimum at 3400–3500 cm^{-1} observed in the sample CC100A could be assigned to the O–H stretch due to the residual moisture [14]. Since CC100A and CC100C did not reveal signatures pertaining to the reactants, it is reasonable to assume that the combustion reaction had proceeded up to completion.

3.4 Characterization of the Powders

The characteristics of the powders obtained in this study viz., bulk density (BD), specific surface area (SSA), X-ray

Table 1 Chemical assay of cerium nitrate

Elements	Na, Al	Ca, Cr, Fe, Zn	Sr, Ba	La	Gd, Eu, Yb
Quantity	2–8 ppm	1–5 ppm	0.1–0.5 ppm	~200 ppb	~50 ppb

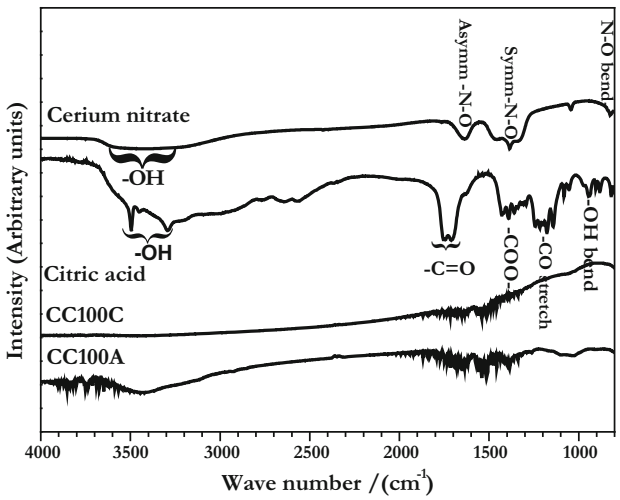

Fig. 1 IR spectra of starting materials and ceria

crystallite size (XCS) and the quantity of the residual carbon are presented in Table 2.

3.4.1 Particle Size Distribution (PSD) and Bulk Density (BD)

The variation in the bulk density of these powders could be represented by expressions (1) and (2).

$$BD_{CC25C} < BD_{CC50C} < BD_{CC75C} \quad (1)$$

$$BD_{CC100C} \cong BD_{CC125C} > BD_{CC150C} \quad (2)$$

The relative distribution of sizes among particles in the powders obtained in this study is presented in Table 3 and the same is graphically represented in Fig. 2. The bulk density of the "calcined" powders was found to be higher than that of the "as prepared" powders. The bulk density of these powders was found to increase with the value of "R". The bulk density increased linearly with R, when the latter was varied from 0.25 to 1.00. Further increase in the value of R to 1.25 and 1.50 did not lead to any significant increase in the bulk density.

The powders CC025C, CC050C and CC075C exhibit a bimodal distribution of particles while a trimodal distribution was observed in the powders CC100C, CC125C and CC150C. In the first three powders with a bimodal distribution, there is a progressive increase in the relative fraction of the coarser fraction when the value of R is increased from 0.25 to 0.75. The increase in the values of the bulk density of these powders could be attributed to the increased quantity of the coarser fraction. The powders CC100C, CC125C and CC150C which exhibited a trimodal distribution, possessed higher bulk densities than the first three. This could be attributed to a better packing in these powders with multiple size fractions. Among these powders CC100C possessed the highest bulk density as compared to CC125C and CC150C. Quite similar to the first three powders, the bulk density of these powders bears a direct correlation with the relative quantity of the fraction with a mean size greater than 100 μm. From the foregoing

Table 3 Size distribution of particles of calcined ceria powders

Sample	Particle size distribution (vol%)		
	10 vol% of sample has size less than (μm)	50 vol% of sample has size less than (μm)	90 vol% of sample has size less than (μm)
CC025C	0.16	16.81	47.04
CC050C	0.17	22.49	57.28
CC075C	0.18	24.66	60.13
CC100C	0.14	22.63	84.36
CC125C	0.10	0.41	50.15
CC150C	0.15	48.66	202.95

Table 2 Characteristics of the ceria synthesized by "gel-combustion"

Sample	CA/NO_3^-	F/M	M/F	Bulk density (Mg m^{-3})		Specific surface area (m^2/g)		X-ray crystallite size by Scherrer method (nm)		X-ray crystallite size by HW method (nm)		Strain ($\times 10^{-3}$)		Residual carbon content (ppm)	
				AP	CP	AP	CP	AP	CP	AP	CP	AP	CP	AP	CP
CC025	0.25	0.75	1.33	0.60	0.62	55.9	22.8	10	24	13	27	2.07	0.36	2137	759
CC050	0.51	1.53	0.65	0.67	0.71	29.9	8.0	11	30	10	34	1.45	0.32	1625	476
CC075	0.76	2.28	0.44	0.75	0.77	19.6	3.8	13	27	19	26	1.91	0.20	1362	304
CC100	1.02	3.06	0.33	0.92	0.95	26.3	11	14	26	16	24	1.14	0.21	1355	626
CC125	1.27	3.81	0.26	0.90	0.94	19.1	10.1	16	26	15	23	0.24	0.34	1148	498
CC150	1.53	4.59	0.22	0.90	0.91	17.9	9.8	17	26	16	26	0.26	0.11	1096	635

CA citric acid, *HW* Hall-Williamsom, *AP* "As-prepared" powder, *CP* calcined powder, *M* $Ce(NO)_3{\cdot}6H_2O$

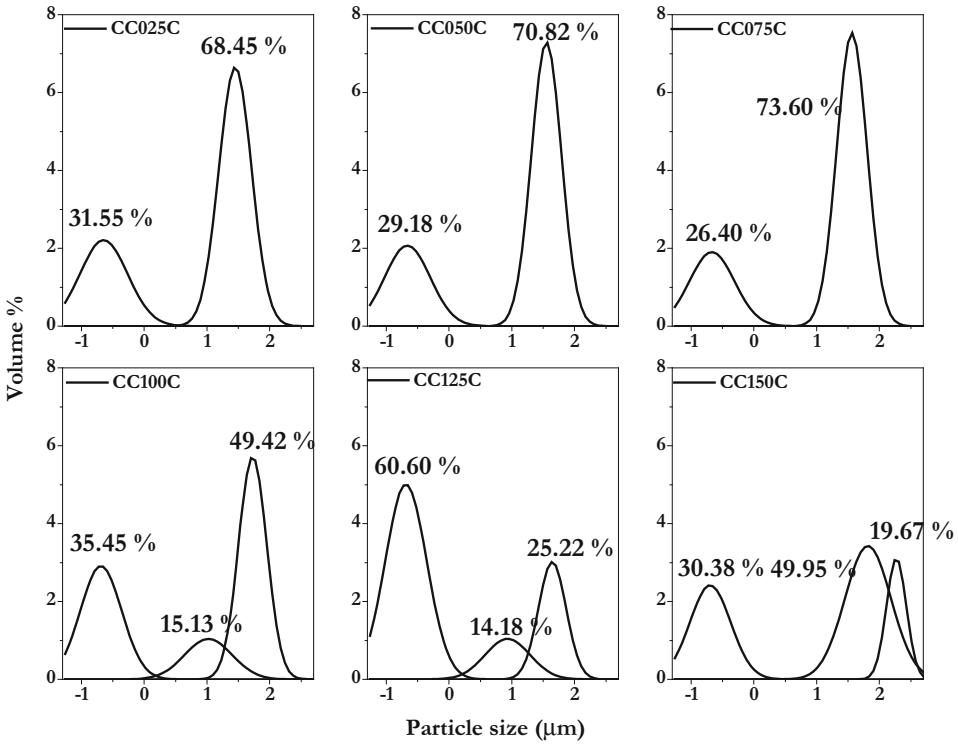

Fig. 2 Size distribution of particles of calcined ceria powders (Peak areas are depicted in percentage)

it is clear that polymodal distribution as well as a higher quantity of the larger size fraction lead to a higher bulk density. In general powders derived through the citrate gel-combustion show a bimodal distribution. The lower size fraction is due to the self attrition of the larger agglomerates. The relative quantities of these two sizes depend upon the strength of these agglomerates. The observations made in this study are similar to those reported by Gu et al. [18] for nanocrystalline ceria obtained by the gel combustion of cerium containing citric acid-glycol mixture.

3.4.2 Specific Surface Area

The dependence of the SSA area of these powders on the value of R is presented in Table 2. It shows that the SSA decreases upon calcination. This could be due grain coarsening during calcination with attendant pore elimination [18]. The specific surface area bears an inverse correlation with the value of R. The SSA of the powders CC025A and CC025C are maximum compared to that of the other products. Gu et al. [18] have obtained powders using citric acid and mixed fuel (citric acid and glycol) with a SSA of 37 m^2 g^{-1} which is comparable to that of powder CC025C (obtained in this study).

Purohit et al. [31] synthesized nanocrystalline ceria from oxalate and hydroxide precursors as well as by using citrate gel combustion. These authors reported a very high value of SSA (127 m^2 g^{-1}) for the citrate gel combustion derived ceria. This value is rather high compared to those reported by others [32]. Further, these authors did not make any attempt to study the systematic dependence of SSA on the value of Chinarro et al. [32] synthesized ceria doped with aliovalent cations (Ca, Sm, Gd, Y) by citrate gel combustion. CC025C was a fluffy, fine powder, the most voluminous among all. During calcination, surface activated sintering would take place leading to a decrease in the SSA of the calcined powder. Chen et al. [17] had observed that salt-assisted synthesis prevents the agglomeration of powders. The specific surface area reported by these authors are significantly higher (about three times more) than the values obtained in the present work.

3.4.3 Residual Carbon

In general, the residual carbon content in the "as prepared" powders tends to increase with the fuel content. In the present study, the residual carbon content decreased with an increase in R. This could be a sampling artifact. However the carbon content of the calcined powder was lower than that of the "as-prepared" powder as expected. Haribabu et al. [14] showed that the presence of residual carbon in the "as prepared" powder was present in the

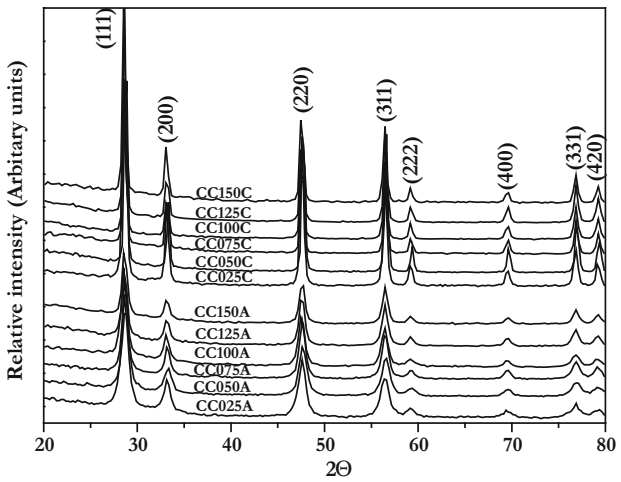

Fig. 3 XRD pertaining to "as-prepared" and "calcined" ceria powders

form of carbonates, which present an IR spectrum similar to those obtained in this study. The quantity of the carbon residue present in the calcined powders was about 300–750 ppm.

3.4.4 Phase Identification and XCS

The X-ray diffractograms (XRD) of the "as-prepared" and "calcined" powders are depicted in Fig. 3. The X-ray crystallite size of the "as-prepared" samples was found to be less than that of the corresponding calcined powders. The crystallite size of all the calcined powders was found to fall in the range of 20–35 nm. A comparison of these diffractograms with the corresponding JCPDS files indicated that the products obtained were fluorite CeO_2 powders. The size of the crystallites ("as prepared" powders) observed in this study is considerably larger than those reported by Purohit et al. [31]. Hwang [15] have reported that nanocrystalline ceria with a crystallite size ranging from 10 to 25 nm could be synthesized by a dry route. However this product comprised a high amount of carbon residue viz., 0.07–2.51 wt%. Yttria doped ceria synthesized by Xu et al. [24] were found to have crystallites with a size range 5–15 nm. However, the TEM analysis of this sample revealed that the crystallite size was in the range of 5–40 nm. From the above it is evident that the powders obtained in this study had reasonably small crystallites and contain minimum carbon residue.

It is evident from this Table 2 that the crystallite size of the "as prepared" ceria powders increased upon calcination. The maximum enhancement in the crystallite size was found for the powders CC050A. The lattice parameters of the calcined powders decreased with an increase in the value of O/Ce (Table 4). However, significant oxygen substoichiometry was not observed in these powders (Fig. 4).

Table 4 Lattice parameter of ceria powders

Sample	Lattice parameter			
	AP (Å)	σ	CP (Å)	σ
CC025	5.40488	0.0784	5.40412	0.0513
CC050	5.39368	0.2033	5.38908	0.1900
CC075	5.40061	0.1078	5.40296	0.0231
CC0100	5.40962	0.0338	5.40545	0.0149
CC0125	5.40521	0.0472	5.4023	0.0380
CC0150	5.40341	0.0515	5.4082	0.0385

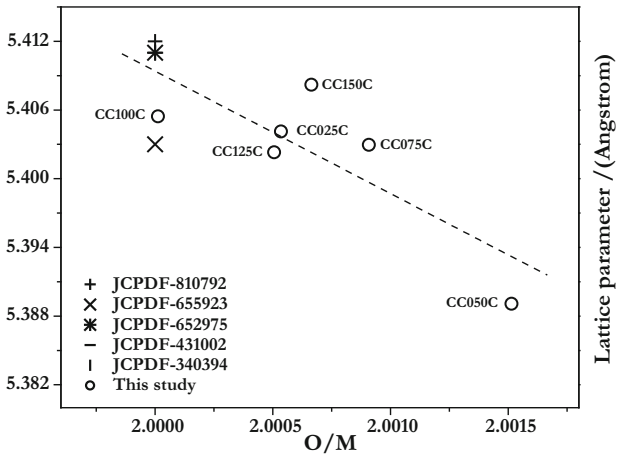

Fig. 4 Variation in the lattice parameter with O/Ce

3.4.5 Microstructural Characterization of CC025C

TEM images of CC025C are depicted in Fig. 5. Selected area electron diffraction (SAED) image pertaining to this sample reveals that this powder comprised nanocrystallites of the dioxide with the fluorite structure. Further it is evident that nucleation and partial grain growth takes place during calcination which is substantiated by the presence of faceted crystallites. Both the bright field as well as dark field images of this sample reveal the presence of crystallites with a size of about 20–50 nm. This is in agreement with the values of crystallite sizes obtained by the HW analysis of the XRD data.

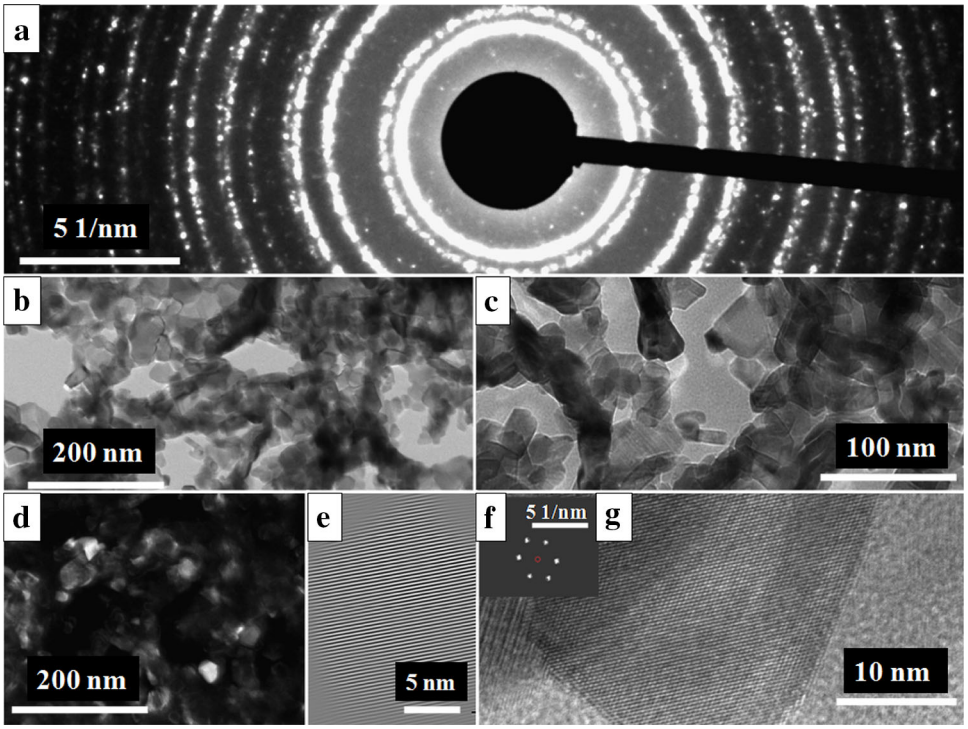

Fig. 5 Microstructural characterization of CC025C powders: **a** SAED image, **b**, **c** bright field images revealing faceted grains, **d** dark field image revealing crystalline characteristics, **e** HRTEM image, **f** IFFT image, **g** typical faceted grain

Table 5 Characteristics of the pellets

Sample	Green density (Mg m^{-3})	% TD	Sintered density (Mg m^{-3})			% Theoretical density		
			1473 K	1673 K	1873 K	1473 K	1673 K	1873 K
CC025C	3.41	47.36	6.84	6.96	7.11	94.34	96.51	98.63
CC050C	3.71	51.32	7.01	6.45	6.82	96.14	89.48	94.55
CC075C	3.88	53.99	7.14	6.60	6.62	98.35	91.46	91.74
CC100C	3.81	52.81	6.98	6.62	6.74	96.26	91.76	93.38
CC125C	3.87	53.71	6.97	6.65	7.02	96.04	92.2	97.30
CC150C	3.91	53.75	6.96	6.70	6.90	96.13	92.86	95.69

TD theoretical density

3.5 Characteristics of the Pellets

3.5.1 Densities of the Green Pellets

The densities of the green pellets (63 MPa) obtained in this study are given in Table 5. There is no significant variation in the green densities of the pellets with an increase in the value of R. Almost all the green pellets exhibited a density of about 50 % TD except CC025C which was found to have the lowest green density of 47 % TD. This reduction in the green density is probably due to increased magnitude of interparticle friction or due to the presence of harder agglomerates in this powder [19]. CC150C yielded pellets with the highest green density as compared to the other powders. Both the presence of multiple size fractions of agglomerates and lower strength of these particles would have helped an efficient compaction leading to a higher green density.

3.5.2 Densities of the Sintered Pellets

The densities of the sintered pellets obtained in this study are given in Table 5 and their variation with temperature is depicted in Fig. 6. A comparison of both the sintered density with bulk density is presented in Fig. 7. The variation in the sintered density with temperature and the

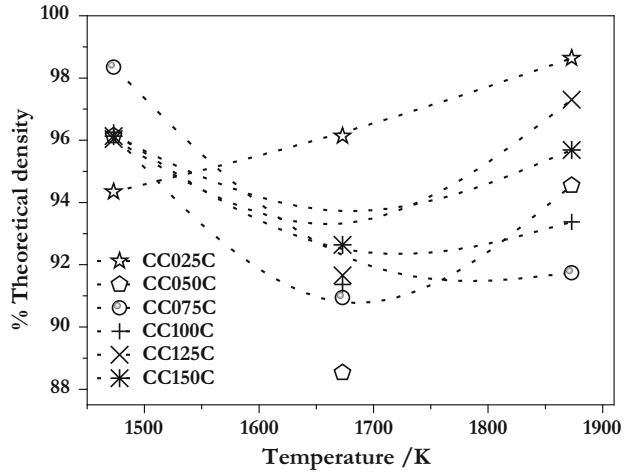

Fig. 6 Dependence of the sintered density on the sintering temperature

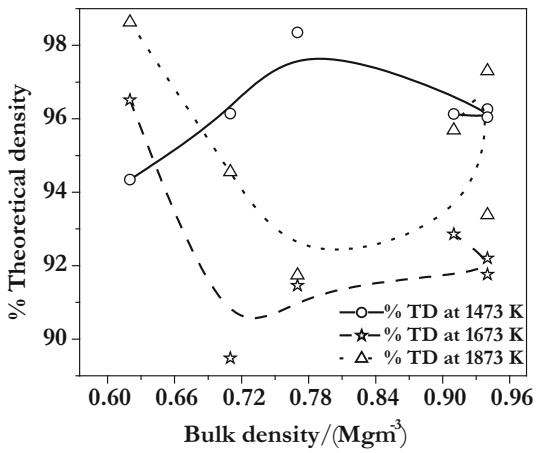

Fig. 7 Correlation between the bulk density of ceria and its sintered density

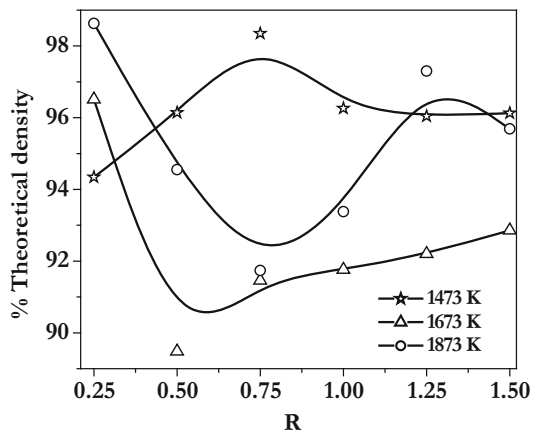

Fig. 8 Variation in the sintered density with the value of R

value of R is given in Fig. 8. The sintered densities of these pellets range from 92 to 98 % TD. The ceria powder CC025C showed a linear increase in the sintered density with the temperature of sintering whereas the others powders showed a complex dependence. The decrease in the sintered density observed at a higher temperature (1673 K) could be due to irregular grain coarsening [33, 34] observed in nanocrystalline ceramics. All the compacts (except CC025C) exhibited a minimum in the values of their sintered density at 1673 K (Fig. 6). Probably the threshold temperature beyond which this phenomenon takes place lies in between 1473 and 1673 K. Further investigations are required in order to find out this threshold temperature.

The maximum sintered density that could be obtained was 98.4 % TD. for the composition CC075C at a temperature as low as 1473 K which is much higher than the values of sintered densities reported by Purohit [31] for the ceria powders obtained through citrate gel combustion. Chyi and co workers [15] had obtained a maximum sintered density of about 92 % TD by sintering nanocrystalline ceria powders at 1523 K. This augurs well with the observation made in this study. Possibly, the threshold temperature beyond which the irregular grain coarsening [33, 34] would have taken place is between 1523 and 1673 K. Further comparison of sintered density of ceria and doped ceria obtained through various methods is presented in Table 6.

4 Conclusion

Free flowing, granular nanocrystalline ceria powders with moderate specific surface area (9.8–22.8 $m^2\ g^{-1}$) and a high sinterability could be produced by the citrate combustion synthesis. The yellow color of these ceria powders deepened with an increase in the R ratio from 0.25 to 1 and remained constant thereafter. The bulk density of the as prepared powders increased gradually with increase in R ratio. The carbon residue present in "as-prepared" powders decreased with an increase in R ratio. However the carbon residue was effectively oxidized during calcination as evidenced by the diminished quantity of residual carbon in the calcined powders. No significant variation in specific surface area was observed with the value of R. It was demonstrated that nanocrystalline powders of ceria with about 25 nm crystallite size and minimum amount of carbon residue could be synthesized by using citric acid as a fuel. The studies on the sinterability of these powders revealed that the threshold temperature beyond which irregular grain coarsening [33, 34] would takes place lies between 1523 and 1673 K. Sintering of powders at 1473 K revealed that the powders obtained with R ratio 0.75 were found to possess highest sintered density (98.4 % TD).

Table 6 Comparison of sintered densities of ceria reported in the literature

Preparation method	Calcination (K)	Pressing method	Sintering temperature		SD (% TD)	Reference
CS (dry route)		CP	1523 K; 1 h		≈92	[15]
CS (Yttria doped)		Uniaxial	O/F	1473 K; 4 h	≈64	[13]
			0.5	1523 K; 4 h	≈70	
				1573 K; 4 h	≈75	
				1623 K; 4 h	≈78	
				1673 K; 4 h	≈83	
			1.0	1473 K; 4 h	≈71	
				1523 K; 4 h	≈77	
				1573 K; 4 h	≈80	
				1623 K; 4 h	≈85	
				1673 K; 4 h	≈89	
			1.5	1473 K; 4 h	≈78	
				1523 K; 4 h	≈86	
				1573 K; 4 h	≈90	
				1623 K; 4 h	≈94	
				1673 K; 4 h	≈95.1	
CS	823 K; 1 h	CP		1523 K; 1 h	≈94	[16]
CD	973 K	Isostatic		1273 K; 2 h	>99	[35]
OD	873 K; 1 h	Uniaxial		1523 K; 1 h	90	[31]
HD				1523 K; 1 h	84	
CS				1523 K; 1 h	96	
CD (Yttria doped)	893 K	Hot pressed		1623 K; 30 min	99.4	[36]
CS (Yttria doped)		Uniaxial		1523 K; 4 h	≈90.5	[24]
				1573 K; 4 h	≈91	
				1623 K; 4 h	≈94	
				1673 K; 4 h	≈95	
				1723 K; 4 h	≈93.5	
OD (mixed oxalate)	623 K			1273 K; 1 h 30 min	83	[37]
OD (rare earth doped)	873 K	CIP		1473 K; 4 h	95	[38]

CS combustion synthesis, *CD* carbonate decomposition, *CP* cold pressed, *HD* hydroxide decomposition, *OD* oxalate decomposition, *CIP* cold isostatic pressing, *SD* sintered density, *O/F* oxidant to fuel ratio

Sintered density of CC025C powders was found to increase linearly with sintering temperature.

Acknowledgments The authors would like to acknowledge Dr. G. Panneerselvam for helping to record the X-ray diffraction pattern. The authors would also like to acknowledge Dr. Amirthapandian of Materials Science Group, IGCAR for recording TEM images.

References

1. Patil K C, Hegde M S, Rattan T and Aruna S T, *Chemistry of Nanocrystalline Oxide Materials: Combustion Synthesis, Properties and Applications*, World Scientific, Singapore (2008).
2. Tsipis E V and Kharton V V, *J Solid State Electrochem* **12** (2008) 1039.
3. Fu Q X, Zha S W, Zhang W, Peng D K, Meng G Y and Zhu B, *J Power Sources* **104** (2002) 73.
4. Zhu W Z, and Deevi S C, *Mater Sci & Eng A* **362** (2003) 228.
5. Kiork R E and Othmer D F, *Encylopedia of Chemistry and Technology*, 3rd ed., Wiley, New York, (1979).
6. Dorr W, Hellmann S, and Mages G, *J Nucl Mater* **140** (1986) 7.
7. Jain A, Ananthasivan K, Anthonysamy S, and Rao PRV, *J Nucl Mater* **345** (2005) 245.
8. Alifanti M, Baps B, and Blangenois N, *Chem Mater* **15** (2003) 395.
9. Zhou Y C, and Rahman M N, *J Mater Res* **8** (1993) 1680.
10. Li Y X, Chen W F, and Zhou X Z, *Mater Lett* **59** (2005) 48.
11. Yin L X, Wang Y Q, and Pang G S, *J Colloid Interface Sci* **246** (2002) 78.
12. Djuricic B, and Pickering S, *J Eur Ceram Soc* **19** (1999) 1925.
13. Xu H, Yan H, and Chen Z, *J Power Sources* **163** (2006) 409.
14. Palneedi H, Mangam V, Das S, and Das K, *J Alloys Compd* **509** (2011) 9912.
15. Hwang C-C, Huang T-H, Tsai J-S, Lin C-S, and Peng C-H, *Mater Sci Eng B* **132** (2006) 229.
16. Purohit R D, Sharma B P, Pillai K T, and Tyagi A K, *Mater Res Bull* **36** (2001) 2711.
17. Chen W, Li F, Yu J, and Li Y, *J Rare Earths* **24** (2006) 434.
18. Gu L, and Meng G, *Mater Res Bull* **42** (2007) 1323.

19. Chandramouli V, Anthonysamy S, and Rao PRV, *J Nucl Mater* **265** (1999) 255.
20. Anthonysamy S, Ananthasivan K, Chandramouli V, Kaliappan I, and Rao P R V, *J Nucl Mater* **278** (2000) 346.
21. Ananthasivan K, Anthonysamy S, Sudha C, Terrance A L E, and Rao P R V, *J Nucl Mater* **300** (2002) 217.
22. Biswas M, Prabhakaran K, Gokhale N M, and Sharma S C, *Mater Res Bull* **42** (2007).
23. Fu Y-P, and Lin C-H, *J Alloys Compd* **389** (2005) 165.
24. Xu H M, Yan H G, and Chen Z H, *Mater Character* **59** (2008) 301.
25. Banerjee S, and Devi P S, *J Nanopart Res* **9** (2007) 1097.
26. Jain S R, Adiga K C, and Pai Vernekar V R, *Combust Flame* **40** (1981) 71.
27. Yuan Q, Duan H-H, Li L-L, Sun L-D, Zhang Y-W, and Yan C-H, *Mater Character* **335** (2009) 151.
28. Biswas M, and Bandyopadhyay S, *Mater Res Bull* **47** (2012) 544.
29. Biswas M, and Bandyopadhyay S, *Adv Powder Technol* **25** (2014) 536.
30. Biswas M, and Bandyopadhyay S, *Ceram Int* **39** (2013) 9699.
31. Purohit R D, Saha S, and Tyagi A K, *Ceram Int* **32** (2006) 143.
32. Chinarro E, Juradon J R, and Colomer M T, *J Eur Ceram Soc* **27** (2007) 3619.
33. Wang X-H, Chen P-L, and Chen I-W, *J Am Ceram Soc* **89** (2006) 431.
34. Deng X-Y, Bai H-L, Zhou H, and Chen I-W, *J Am Ceram Soc* **89** (2006) 438.
35. Li J-G, Ikegami T, Wang Y, and Mori T, *J Am Ceram Soc* **85** (2002) 2376.
36. Dragoo AL, and Domingues L P, *J Am Ceram Soc* **65** (1982) 253.
37. Overs A, and Riess I, *J Am Ceram Soc* **65** (1982) 606.
38. Higashi K, Sonoda K, Ono H, Sameshima S, and Hirata Y, *J Mater Res* **14** (1999) 957.